

Prediction of crucial interactions for icosahedral capsid self-assembly by energy landscape atlasing

Ruijin Wu¹, Rahul Prabhu¹, Bennett, Antonette², Aysegul Ozkan¹, Mavis Agbandje-McKenna², Meera Sitharam^{1,*}

1 Department of Computer and Information Science and Engineering, University of Florida, Gainesville, Florida, United States of America

2 Department of Biochemistry and Molecular Biology, University of Florida, Gainesville, Florida, United States of America

* E-mail: sitharam@cise.ufl.edu

Abstract

We predict crucial inter-atomic interactions between monomers for the autonomous assembly of three icosahedral viral capsids, Adeno Associated Virus type 2 (AAV2), Murine Parvo Virus (MVM), and Bromo Mosaic Virus (BMV), by approximating changes in the partition function of the capsid assembly landscape when an interaction is removed. At the interface-scale, the partition function computation uses *atlases* of selected subassembly landscapes for each interface type and their abbreviated *bar-codes*. The first (direct) prediction of cruciality of an interaction for successful capsid assembly assumed the interface assembly is essential for capsid assembly. The interface-scale prediction was blind to the mutagenesis data used for validation.

The atlases are generated by the geometric method and curated opensource software EASAL (efficient atlasing and search of assembly landscapes), whose input consists of (a) the monomer geometry - atom coordinates; and for each interface type, (b) pair potentials for a candidate set of interactions along with Van der Waals sterics, and (c) structure of selected, small subassemblies. The method comes with rigorous accuracy-efficiency trade-off estimates.

A second two-scale measure of cruciality of interactions and residues for capsid assembly is obtained as follows. Combinatorial entropy is used to define the cruciality of an interface for successful assembly of the capsid. This is combined with the interface-scale prediction using statistical learning. The learning algorithm uses - for training - a fraction of the mutagenesis data, with the remainder of the data being used for validation. By reliably and rapidly narrowing down target interactions, these in-silico predictions can inform and reduce the time spent on time-consuming in-vitro and in-vivo experimentation.

1 Introduction

Icosahedral viral capsid assembly from almost identical monomers is primarily driven by inter-atomic interactions at interfaces between monomers. Icosahedral symmetry restricts the interface types to a small set. To predict the cruciality of a specific interaction and participating residues for successful capsid assembly, we analyze the viral capsid assembly landscape at two scales, the interface-scale and the capsid-scale.

At the interface-scale, we determine the cruciality for successful subassembly across an interface by approximating the changes in the partition function when the interaction is removed. We use two ways to measure change in the partition function for a given small subassembly across a given interface. The first uses the partition function for all the minimal energy regions, representing all the stable subassembly configurations. The second uses the normalized partition function for the potential energy basin corresponding to the specific subassembly configuration occurring in the successfully assembled capsid. This estimates the probability that a stable configuration is in fact the successful subassembly configuration. We use the ratio of each of these measures with and without an interaction - averaged over selected small subassemblies across an interface - to measure cruciality of that interaction for that interface.

The change in partition function is approximated using an *atlas* of the assembly landscape, generated - with minimal sampling - by the geometric method and curated opensource software EASAL (efficient atlasing and search of assembly landscapes, see software [1], video [2] and user guide [3]) [4–6]. The input to EASAL consists of (a) the monomer geometry - atom coordinates; and for each interface type, (b) pair-potentials for a candidate set of assembly-driving interactions along with Van der Waals sterics, and (c) small subassembly structures extracted from known capsid structure. An atlas is a partition of the assembly landscape into contiguous region of nearly equipotential energy called *active constraint regions* or *macrostates*, organized as a refinable, queryable roadmap, that can further be abbreviated as a *bar-code*. The constraints are the pair-potentials as in (b) above. The active constraint regions are analyzed using combinatorial graph rigidity, whereby the effective dimension of a macrostate becomes a proxy for its energy level. The methodology comes with rigorously proven accuracy-efficiency trade-offs.

Our first, interface-scale predictions were completely blind to the experimental data that were used for validation. Although generalizing an interface-scale prediction to the capsid-scale assumes the necessity of that interface for capsid assembly, our interface-scale predictions were validated successfully using mutagenesis data towards capsid assembly disruption.

Our second prediction additionally incorporates the cruciality of an interface for capsid assembly. The dimension of the capsid assembly landscape - involving several interfaces (60 for $T = 1$ and 180 for $T = 3$) - makes direct computations intractable. Hence, we treat the capsid as being recursively assembled from stable subassemblies at interfaces [7]. The likelihood of such an *assembly tree*, given successful capsid assembly, is a measure of combinatorial entropy. This depends both on the stability and formation rates of the intermediate subassemblies, and the number of equivalent assembly trees under icosahedral symmetry [8–10]. The cruciality of an interface for successful capsid assembly is then determined by assembly trees that involve that interface. The relative weights of the three cruciality measures described above, two at the interface-scale and one at the capsid-scale, are then determined by statistical learning. The learning algorithm uses - for training - a small fraction of the mutagenesis-based experimental data towards assembly disruption, to learn the parameters of the statistical model. The remainder of the mutagenesis data is used to validate the cruciality of residues in three viruses, Adeno Associated Virus (AAV), Murine Parvo Virus (MVM), and Bromo Mosaic Virus (BMV).

1.1 Motivation and related work

Viral capsid self-assembly is a critical part of the viral life-cycle. Understanding the process of assembly illuminates the pathophysiology of infectious diseases and allows us to target assembly processes with drugs and vaccines. Like most other supramolecular assemblies that occur widely in nature, viral capsid self-assembly is an extremely robust, rapid, and spontaneous process. Spontaneity makes it difficult to control in vitro, rapidity makes it difficult to get snapshots of the process, and robustness makes it difficult to isolate crucial combinations of assembly-driving interactions (see Fig. 1).

A key component in understanding the virus assembly process is identifying those *crucial interactions* whose removal disrupts assembly. In a wet lab, specific residues can be mutated to disable all interactions involving these residues. This method is called *mutagenesis analysis*. The effect of the mutation on assembly efficacy is measured by the concentration of successfully assembled viral capsids using one of the following experimental studies: cryo-electron microscopy, NMR spectroscopy, calorimetric studies, or in vitro systems for measuring rates and concentrations [11]. Many of these experimental methods are laborious and time consuming. For instance, performing mutagenesis on less than 100 residues on a single virus, followed by cryo-electron microscopy to analyze the concentrations of sub-assemblies takes years. This makes taking blind alleys into experiments extremely expensive. Thus, there is a need for rapid and reliable mathematical and computational tools for supramolecular assembly that can inform further experimentation.

At the interface-scale, supramolecular assembly is affected by the configurational entropy of small assemblies at the inter-monomeric interfaces, driven by weak forces and non-covalent bonds. However, full-blown computation of configurational entropy is a notoriously difficult problem. All prevalent methods rely on effectively computing the volumes of assembly landscape regions, typically by sampling [12–14], which is prohibitive due to the high dimension of the assembly landscape. By contrast, EASAL is able to approximate the configurational entropy of small assembly system using an atlas bar-code, without relying

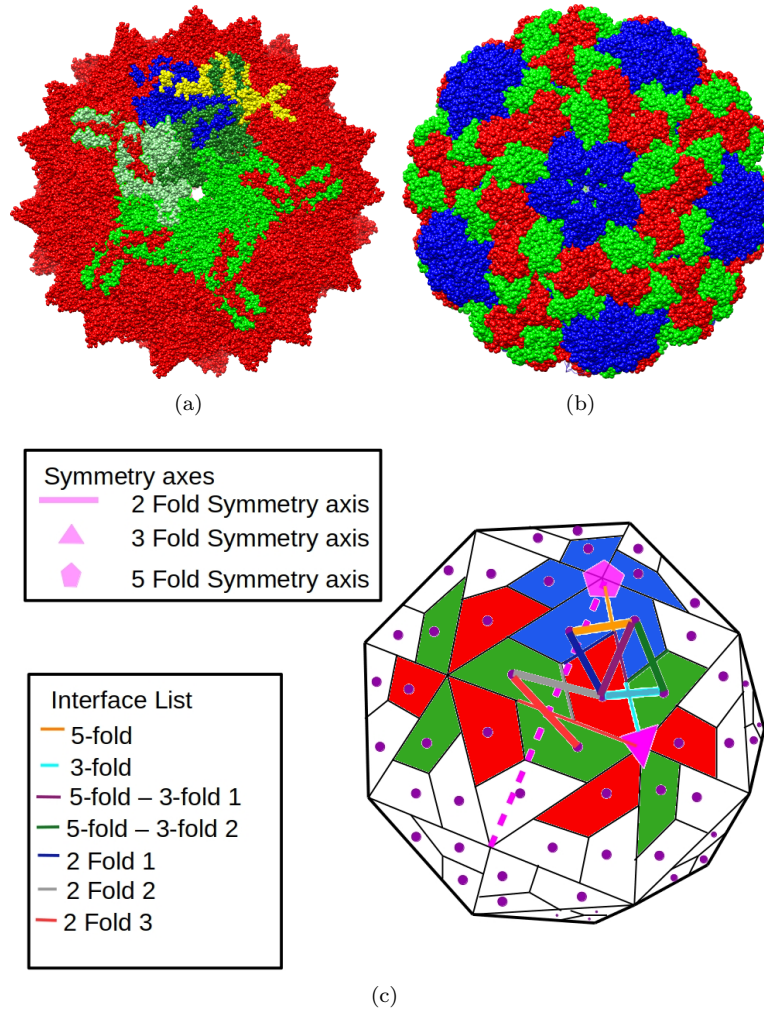


Fig 1. (a) X-ray structure of a $T = 1$ virus (AAV2) showing its 3 types of interfaces. See Section 1.1. Monomers at the 5-fold interfaces are colored shades of green, light green and blue form a 2-fold interface assembly, and dark green, blue and yellow pairwise form 3-fold interface assemblies. (b) X-ray structure of a $T = 3$ virus (BMV) showing 3 types of monomers (green, blue, and red). (c) A cartoon of a $T = 3$ virus showing the 3 types of monomers (green, blue, and red) and 7 types of interfaces, along with the 3 different types of symmetries (shown in pink).

heavily on sampling, thereby ameliorating the curse of dimension, as shown using rigorous complexity analysis and computational experiments [6].

High geometric or topological complexity of the assembly landscape (disconnectedness, channels of varying effective dimension etc.), means that sampling techniques like Monte Carlo and Molecular Dynamics can only claim stochasticity and uniform sampling in the limit, i.e., when they run for sufficiently long or start from sufficiently many initial configurations [15–20]. On the other hand, methods based on principal component analyses of the co-variance matrices from a trajectory of samples in internal coordinates generally overestimate the volumes of assembly landscape regions. EASAL, on the other hand, uses the novel geometric idea of convexifying *Cayley* parameters to represent macrostates, which avoids gradient descent used by the above-mentioned methods, thereby increasing sampling efficiency.

Ab initio methods such as [21], based on geometric algebras are used to give bounds or to approximate configurational entropy without relying on Monte Carlo or Molecular Dynamics sampling. However, it is not clear how to extend them beyond restricted assembly systems such as a chain or loop of rigid molecular components, each consisting of at most 3 atoms, where each component is non-covalently bound to their neighboring components at exactly 2 sites. EASAL on the other hand is applicable more generally to assemblies with larger inputs.

While for small assemblies it is possible to atlas the assembly landscape and compute the entropy directly, for larger assemblies, such as virus capsid systems (consisting 60 monomers for $T = 1$ and 180 monomers for $T = 3$ viruses), the assembly landscape is too big to be atlased directly. Therefore, to tractably deal with the high dimension of their assembly landscape, larger assemblies are typically treated as being recursively assembled as an interface assembly system, from a small number of stable intermediate subassemblies [7]. The assembly model [22] based on the local-rules theory [23–26] computes the combinatorial entropy considering both the number of different assembly way and the microscale kinetics at each assembly stage. However, it relies crucially on the simplified representation of the monomers and their geometric interactions.

Several computational studies have been conducted on various aspects of the virus life cycle. [27] uses rigidity analysis on the fully assembled capsids of icosahedral proteins to identify functional units of the capsid. Assembly pathways have been used to study the self-assembly of polyhedral systems from identical sub-units; for example, [28] study the role of assembly pathways and the degrees of freedom of intermediate sub-assemblies in the self-assembly of polyhedra with known isomers. The goal is to manipulate the degrees of freedom of the intermediate sub-assemblies to increase the concentration of one isomer over others. In contrast, our paper uses graph and rigidity analysis to study and synthesize combinatorial and configurational entropy of virus capsid assembly. Specifically we use assembly pathways of viral capsids with the goal of identifying interfaces whose removal causes disruption to assembly.

Organization: The rest of the paper is organized as follows. The methods Section 2 describes the two-scale method of computing the cruciality of inter-atomic interactions between monomers to the interface and the capsid assembly as a whole. The results Section 3 provides the results validating the cruciality prediction of interactions to the capsid, in three viruses, AAV, MVM and BMV.

2 Materials and methods

In Section 2.1, we discuss some background on the configurational entropy of virus capsid assembly. In Section 2.2, we describe key features of the EASAL methodology (see software [1], video [2] and user guide [3]). In Section 2.3 we discuss the combinatorial entropy in viruses.

In Section 2.4 we describe the computation of the cruciality of inter-atomic interactions across monomers to interface subassembly and thereby to capsid assembly. In Section 2.5 we describe a second type of cruciality of interfaces to capsid assembly. In Section 2.6 we describe statistical models to combine the interface-scale configurational entropy and the capsid-scale combinatorial entropy to predict the cruciality of an interaction at the capsid level.

2.1 Background: configurational entropy in virus assembly

The efficacy of viral capsid assembly is largely due to the structure of its equilibrium free energy landscape. Specifically, the depth and volume of the potential energy basins, including the basin containing the successfully assembled capsid configuration. The free energy at a basin depends on the average potential energy and the configurational entropy of the basin. Of these, the computation of the configurational entropy dominates the computation of free energy.

Let $E(x)$ be the potential energy function, defined over the assembly landscape, for an assembly configuration x (the function E is described in detail in 2.2). The partition function Q is an integral over the energy basin β , given by

$$Q = \int_{\beta} e^{\frac{-E(x)}{k_B T}} dx$$

where $x \in \beta$ is a configuration in the basin, k_B is the Boltzmann's constant and T is the absolute temperature. The configurational entropy S of the basin is

$$S = k_B \ln Q + \frac{\langle E \rangle}{T}$$

where $\langle E \rangle$ is the average energy over the basin.

The free energy F of a system with a single energy basin β is given by:

$$F = \langle E \rangle - TS$$

Hence, over a region C of constant energy E_C , for example an active constraint region as defined in EASAL, the entropy is merely a function of the volume V_C of the region.

$$S_C = k_B \ln V_C \tag{1}$$

where $V_C = \int_C dx$.

In a landscape with multiple potential energy basins β_i , each of which has a constant energy E_i , the partition function of each energy basin Q_i can be expressed as a weighted sum of the volumes V_i of the different basins.

$$Q_i = \int_{\beta_i} dx \cdot e^{\frac{-E_i}{k_B T}} = V_i \cdot e^{\frac{-E_i}{k_B T}} \tag{2}$$

The normalized partition function p_i is the probability of finding the system in the energy basin β_i :

$$p_i = \frac{Q_i}{\sum_i Q_i} \tag{3}$$

In next section we show how to approximate the computation of the partition function by generating an atlas of the capsid assembly landscape using EASAL and extracting a relevant bar-code.

2.2 Atlasing and entropy computation using EASAL

An *interface assembly system* (see Fig. 1) consists of (a) the monomer geometry - atom coordinates; and for each interface type, (b) short-range Lennard-Jones potentials for a candidate set of interactions, i.e., atom pairs (one from each monomer) along with Van der Waals sterics, and (c) small subassembly structures extracted from successfully assembled capsid.

The potential energy $E(x)$ for an *interface assembly configuration* x has one Lennard-Jones term for each atom pair (one from each monomer). In EASAL, the short-range Lennard-Jones pair potentials are *geometrized* by discretizing into three intervals: large distances at which Lennard-Jones potentials are no longer relevant, contributing E_h to the potential energy of the configuration; short distances prohibited by Van der Waals forces; and interval between the two known as the Lennard-Jones *well*, contributing E_l to the

potential energy of the configuration. We say that a pair of atoms has an *active constraint* if the distance between their centers is within the discretized Lennard-Jones well.

For a landscape with N Lennard-Jones terms, potential energy of a configuration with N_a active constraints is given by:

$$E = N_a E_l + (N - N_a) E_h = N E_h - N_a (E_h - E_l) \quad (4)$$

In the expression for partition function in Eq. 2, each configuration contributes a weight

$$e^{\frac{-E}{kT}} = e^{\frac{-N E_h + N_a (E_h - E_l)}{kT}} = C \cdot \left(e^{\frac{E_h - E_l}{kT}} \right)^{N_a}$$

where $C = e^{\frac{-N E_h}{kT}}$ is a constant of the landscape and is canceled out when calculating the normalized partition function, and the weight

$$w(N_a) = \left(e^{\frac{E_h - E_l}{kT}} \right)^{N_a} \quad (5)$$

With this geometrization of energy, the potential energy basin is completely determined by its partition into *active constraint regions*, i.e., regions of the assembly landscape whose configurations have a particular set of active constraints and hence, nearly constant potential energy. This gives a queryable *roadmap* of the basin, where each region is uniquely labeled by an *active constraint graph*, whose edges are the active constraints and whose vertices are the participating atoms. Using combinatorial rigidity [29], each active constraint generically reduces the effective dimension of the region by one. The bottom of each basin is a 0-dimensional region R , with active constraint graph G , containing the minimum energy configurations. The higher energy regions leading to R are exactly those that have active constraint graphs that are subgraphs of G .

One of EASAL’s key features is the generation of roadmaps for all basins, called an *atlas*, without relying heavily on sampling (see Fig. 2). This is achieved by using a recursive method that searches the interior of higher energy regions for boundary regions with exactly one new active constraint. Searching for such boundary regions (which are effectively of one fewer dimension) has a higher chance of success than looking for the lowest energy - which are the lowest dimensional active constraint regions - directly.

Staying within active constraint regions is achieved by a second key feature of EASAL: *convexifying* active constraint regions using customized, distance-based or *Cayley* parametrization, avoids gradient-descent to enforce active constraints, and results in high efficiency search with minimal sampling and reducing repeated or discarded samples. In addition, it is straightforward to compute the inverse map from the Cayley parameter values to their corresponding finitely many Cartesian configurations. Cayley convexification leverages geometric features that are unique to assembly (as opposed to protein folding). Together, the active constraint regions, their effective dimensions, and their volume approximations obtained through Cayley parameterization, provide an abbreviated atlas *bar-code* for the basin structure of the assembly landscape.

2.3 Background: combinatorial entropy in virus assembly

Combinatorial entropy of the capsid assembly captures the number of possible ways in which a successful assembly configuration can be recursively decomposed into subassemblies down to the rigid motifs in the monomers [7–10]. In reverse, larger assemblies are treated as being recursively assembled as interface assembly systems. Since the monomers that are far away from the interface tend to have little impact on the assembly, we can simplify the participants of each interface assembly system to monomers or dimers near the interface.

As shown in Fig. 3, there is typically more than one way of treating a subassembly as an interface assembly. When there are multiple interfaces to choose from, we consider the free energy and reaction rates of each of the options and pick the best interface for the subassembly.

With this setup, we define a labeled binary tree, called an *assembly tree*, to describe how a series of subassemblies leads to a full capsid assembly. In an assembly tree, the root node is a successfully assembled viral capsid, and the leaves are monomers. Every internal node of the tree is a subassembly, labeled by its best interface (as defined earlier). Fig. 3, shows an assembly tree for a $T = 3$ viral capsid. Given the

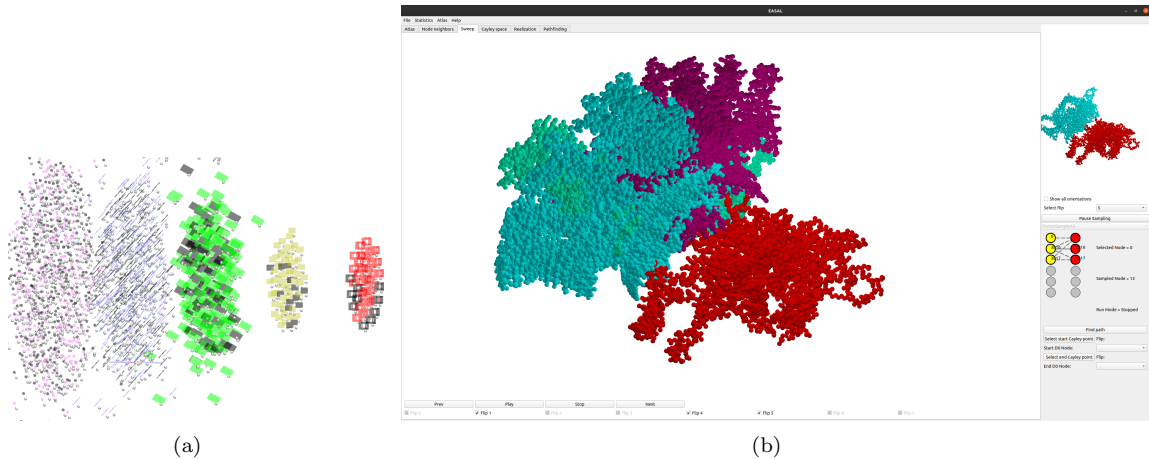


Fig 2. (a) Atlas with changes when an interaction is disabled. See Section 2.2 and Section 2.4. Active constraint regions (nodes of the atlas) of different dimensions are shown in different colors, with red nodes representing regions with 2 active constraints, or 4 effective dimensions, and each of the successive strata (from right to left) showing regions of one more active constraint, or one lower energy level or effective dimension. The left most are the 0-dimensional or lowest energy regions, each of which is the bottom of a potential energy basin, with all its ancestor regions participating in the basin. The black nodes are the active constraint regions that disappear from the atlas due to the removal of a candidate inter-atomic interaction. (b) Screenshot of the EASAL software showing all configurations in an active constraint region of the atlas of the interface assembly system of the two monomers shown on top right. The region's active constraint graph is shown at bottom right, with red and yellow representing atoms in different monomers, the single bold edge representing a single active constraint or interaction c , and the dashed lines representing the 5 Cayley parameters that are used to convexify this effectively 5-dimensional region. On the main screen, the red monomer is held fixed and all of the the second monomer's relative positions (satisfying the one active constraint c) are shown in two sweeps, blue and purple. The 3 different colors (cyan, green and purple) of the second monomer sweeps represent distinct orientations within the same active constraint region.

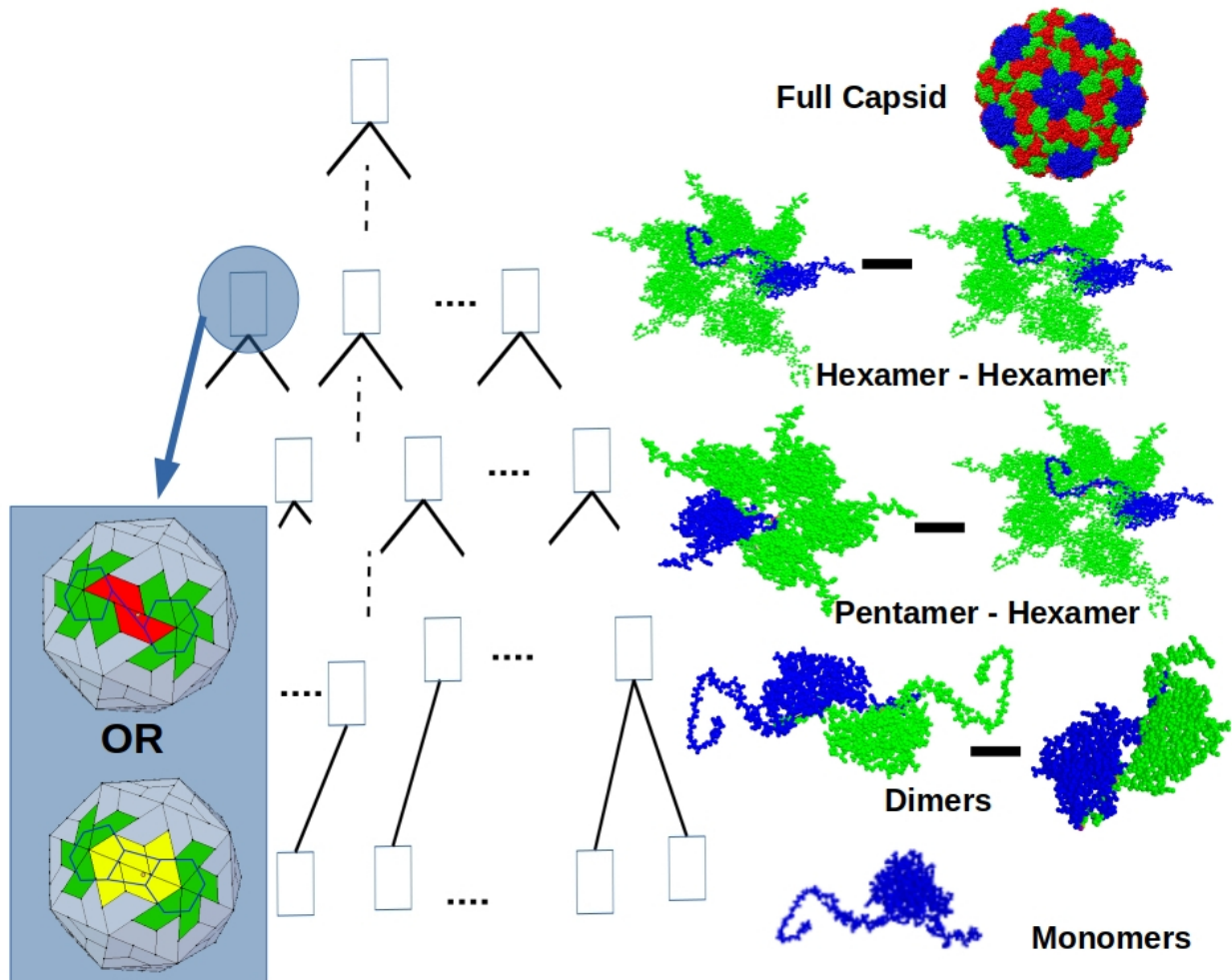


Fig 3. An assembly tree of a $T = 3$ viral capsid. See Section 2.3. The root node represents a successfully assembled viral capsid. Each internal node represents an interface assembly system that contains a stable subassembly configuration that is part of the known, successfully assembled capsid configuration. Children of a node are the participating multimers for the node's interface assembly system. The leaf nodes represent the monomers. To the right of the nodes are their candidate stable subassembly configurations taken from the $T = 3$ BMV X-ray capsid structure. At internal nodes, a choice is made between more than one candidate interface assembly system. On the left we highlight an internal node with 2 available choices for hexamer-hexamer interfaces, of which one is chosen: the inset shows the choices - a single dimer interface highlighted in red; and two dimer interfaces, highlighted in yellow.

free energy and reaction rate of each subassembly and the structure of the assembly tree, we can define its likelihood under the assumption of successful assembly.

An *assembly pathway* is a collection of assembly trees that satisfy some prediction-related criteria [8–10]. For example, all assembly trees that are in one equivalence class under icosahedral symmetries can be grouped as a single assembly pathway. As another example, an assembly pathway can be defined as the collection of such symmetry classes that do not use specific types of interfaces. The papers [8–10] enumerate assembly pathways and compute their likelihood for such criteria.

2.4 Interaction cruciality at interface-scale

We use the atlas generated by EASAL to compute two quantities for each interface assembly landscape: (a) the partition function for minimal energy regions (basin bottoms), and (b) the normalized partition function for the potential energy basin corresponding to the known (successful) interface subassembly configuration called the *true realization*. These two parameters serve as an atlas bar-code to determine the cruciality of interactions at the interface-scale.

As mentioned earlier, the bottom of each basin is a 0-dimensional region R , with active constraint graph G , containing the minimum energy configurations. The higher energy regions leading to R are exactly those that have active constraint graphs that are subgraphs of G . Fig. 4 illustrates, using EASAL screenshots, the basin structure of the of two monomers assembling across a hexamer interface in BMV.

Two assembly configurations are considered distinct if and only if their *similarity* distance (the 2-norm distance between their point coordinate vectors) is at least ε . The number of distinct Cartesian configurations in a region then becomes an approximate measure of the size or volume of the region (configurational entropy associated with that region).

For any interface assembly system s , since the energy of all 0-dimensional configurations is the same, we approximate the sum of the Q_i 's in Eq. 2, with the number of distinct configurations in the union - denoted by R_0^s - of all the 0-dimensional active constraint regions. Formally, the *partition function for all minimal energy regions* of the atlas of a given interface assembly system s is denote it by

$$\nu_{\text{minima}}^s := |R_0^s| \tag{6}$$

The approximation to the normalized partition function of Eq. 5 is the ratio of the number of distinct 0-dimensional configurations in the basin of the true configuration (we call this set R_{true}^s) to ν_{minima}^s . This approximates the probability that the assembly process ends in the true configuration. To improve this approximation we weight each configuration x inversely to its proximity to a higher energy region A by the weight $w(N_a(x))$ of Eq. 5, where $N_a(x)$ is now the number of active constraints in the configurations in A .

Thus the normalized partition function for the potential energy basin corresponding to a successful interface assembly configuration is computed using Eq. 3 as follows:

$$\nu_{\text{capsid}}^s := \frac{\sum_{\mathbf{x} \in R_{\text{true}}^s} w(N_a(\mathbf{x}))}{\sum_{\mathbf{x} \in R_0^s} w(N_a(\mathbf{x}))} \tag{7}$$

Finally, these quantities are used to define our measure of *cruciality of a given input inter-atomic interaction r for a given interface assembly system s* to result in a given true configuration. First we define $\nu_{\text{minima}}^{r,s}$ and $\nu_{\text{capsid}}^{r,s}$ as the same quantities in Eq. 6, and Eq. 7, respectively, obtained by restricting to a portion of the atlas, i.e., those regions where r is not an edge in the active constraint graph (see Fig. 2 and Fig. 4). Now, the *cruciality bar-code* is defined as:

$$\left(\mu_{\text{minima}}^{r,s} := \frac{\nu_{\text{minima}}^{r,s}}{\nu_{\text{minima}}^s}, \mu_{\text{capsid}}^{r,s} := \frac{\nu_{\text{capsid}}^{r,s}}{\nu_{\text{capsid}}^s} \right) \tag{8}$$

Accounting for multimers assembling at an interface:

In a capsid assembly tree, the subassembly at an interface could involve either a monomer pair or a multimer pair. Although the pair potentials at the interface are specified between the monomers closest to the interface,

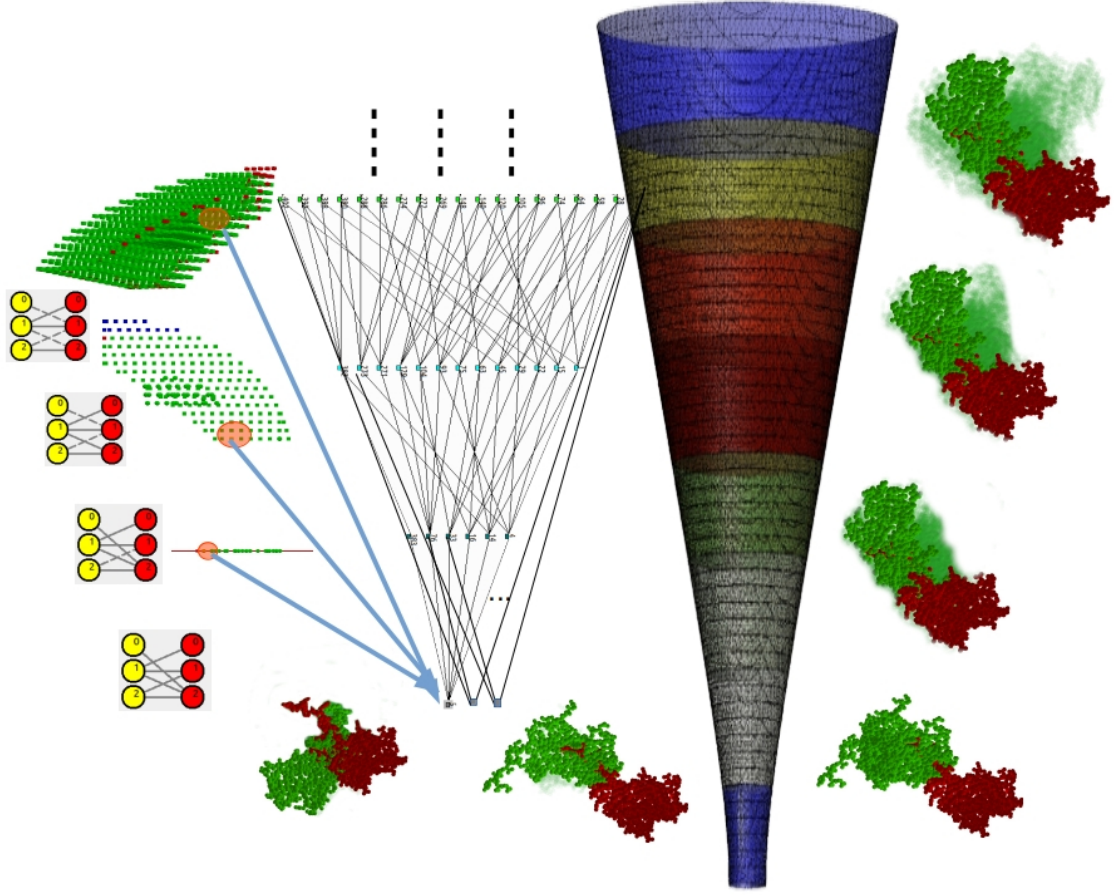


Fig 4. Prediction using *cruciality bar-codes* of Section 2.4 for two monomers assembling across a hexamer interface in BMV. Each node in the atlas roadmap in the middle represents an active constraint region (macrostate) in EASAL. Example active constraint graphs are shown at far left: the yellow and red circles represent atoms participating in active constraints (interactions) in the two monomers. At each successive level, the number of active constraints increases by 1 and the energy level and effective dimension decreases by 1. The atlas nodes in the bottom-most row represent the 0-dimensional, lowest energy, stable assembly configurations; example configurations shown below them. Their total number (for a given interface s , on removal of a given interaction or constraint r) gives $\nu_{\text{minima}}^{r,s}$ in the computation of the cruciality bar-code. Each such configuration together with nearby higher-energy configurations in all of their ancestor nodes constitute one potential energy basin. Their sum, across all basins, weighted by energy level gives the denominator of $\nu_{\text{capsid}}^{r,s}$. The rightmost of the stable assembly configurations at the bottom corresponds to the *true realization*. Above it, the 3 solid configurations and the transparent sweeps around them show the closest configurations to the true realization in successively higher energy regions in its basin (one region each for 3 energy levels shown). To the far left, these sweeps are shown as orange highlights in the corresponding Cayley parameterized regions. The colorful basin plot shows the total weighted configurations in the true basin, stratified by dimension or energy level. Their sum is the numerator of $\nu_{\text{capsid}}^{r,s}$.

each monomer could be part of a multimer whose atoms influence the interface assembly landscape through Van der Waals sterics. We have found that for larger multimers the steric contribution from the monomers far from the interface is negligible and that it is sufficient to consider those interface assembly systems involving certain monomer-dimer pairs selected as follows.

The *dual graph* of a virus capsid is obtained from the icosahedrally symmetric *capsid polyhedron*, with one face per monomer, where interfaces are represented by adjacent faces. See Fig. 5. There is one vertex of the dual graph corresponding to each face of the capsid polyhedron and an edge between two vertices if the corresponding faces are adjacent. For the interface represented by the edge ab in the dual graph, we consider

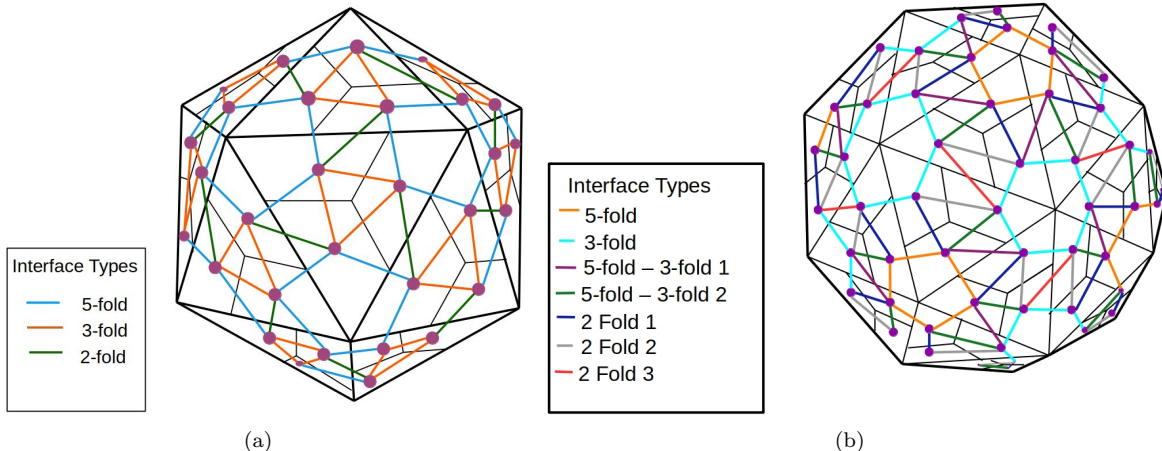


Fig 5. The dual graphs of $T = 1$ and $T = 3$ capsid polyhedra. Faces of the capsid polyhedra are shown with black edges and the colored edges give the dual graph. See Section 2.4.

each triangle abc , and generate 3 atlases with the following assembly systems s : (i) with monomers a and b , (ii) dimer ac and monomer b , (iii) with dimer bc and monomer a . For the 3 $T = 1$ interface types, this gives 9 assembly systems, and for the 7 $T = 3$ interface types, this gives 31 assembly systems.

Now, $\mu_{\text{minima}}^{r,s}$ and $\mu_{\text{capsid}}^{r,s}$ are computed using the atlases for the 3 assembly systems s for the same interface ab , and then averaged to get cumulative values. These are denoted μ_{minima}^r and μ_{capsid}^r and are used to measure the cruciality of the interaction r to the interface ab .

2.5 Interface cruciality at capsid-scale

As mentioned in Section 2.3, given the free energy and reaction rate of each subassembly of all the nodes and the structure of the assembly tree, we can define its likelihood under the assumption of successful assembly and we can group assembly trees into assembly pathways based on prediction-related criteria [8–10]. To simplify our model, we abbreviate the notion of the assembly pathway, to a *connectivity pathway*, which only requires a test of connectivity for the internal nodes of the assembly tree.

Informally, a *connectivity pathway* corresponds directly to a minimal set of interfaces that a successfully assembled capsid must contain to even be a connected structure. It consists of the icosahedral symmetry classes of assembly trees that use only this minimal set of interfaces, weighted by the number of trees.

Given the dual graph $G = (V, E)$, of the capsid polyhedron (defined in Section 2.4), E can be partitioned into sets E_ι , one for each interface type ι (for $T = 1$ capsid polyhedra, there are 3 interface types and for $T = 3$ capsid polyhedra, there are 7 interface types as shown in Fig. 5). A set I of interface types is a *connectivity pathway* if the set of edges $E_I := \bigcup_{\iota \in I} E_\iota$, is a connected subgraph of G and for each $\iota \in I$ $E_I \setminus E_\iota$ is not connected.

Given the small number of interface types for a capsid polyhedron of any T number, we can find all connectivity pathways using a simple graph algorithm. Fig. 6, shows various sets I of interface types, for a

$T = 1$ capsid polyhedron, some of which correspond to connectivity pathways and some that do not. Fig. 7 shows the same for a $T = 3$ capsid polyhedron.

The *cruciality of an interface type* is the number of connectivity pathways containing that interface type.

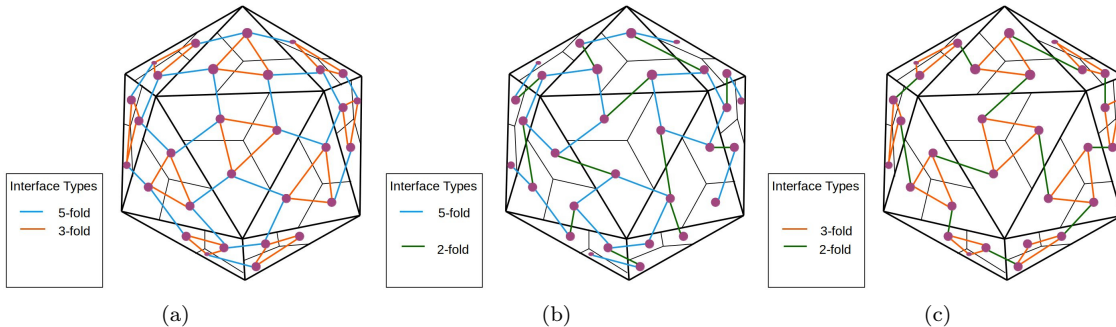


Fig 6. $T = 1$ capsid polyhedra showing all 3 possible connectivity pathways. See Section 2.5.

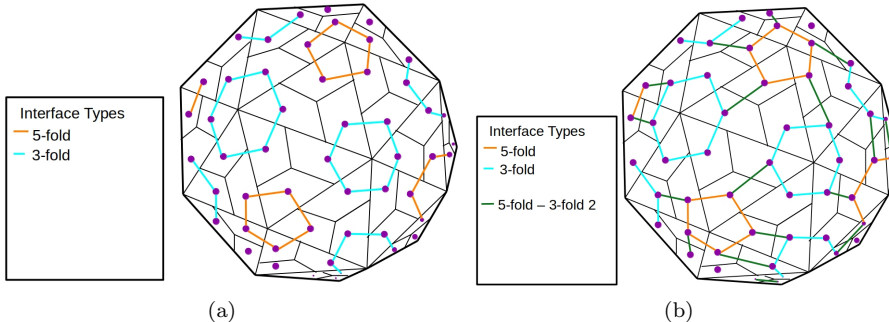


Fig 7. $T = 3$ capsid polyhedra. (a) Only the 5 fold and 3 fold interfaces are shown. This does not correspond to a connectivity pathway. (b) 5 fold, 3 fold and 5 fold-3 fold 2 interfaces are shown. This corresponds to a connectivity pathway. See Section 2.5.

2.6 Two-scale prediction: interaction cruciality at capsid-scale

We use two different types of two-scale predictions. The first prediction assumes that all interface types are equally important and is based only on the cruciality of interactions to interface types. For an interface of type ι , the probability P_ι^r of breaking the interface when dropping an interaction r is measured by the the cruciality bar-code: $(\mu_{minima}^r, \mu_{capsid}^r)$, as described in Section 2.4. Results validating these predictions are shown in Section 3.2.

For the second two-scale prediction, we combine the interaction cruciality at the interface-scale and the interface cruciality at the capsid-scale using a statistical model as follows.

A simple linear model is used to learn the relative weights a_ι , b_ι , and c_ι for

$$P_\iota^r = \sigma(a_\iota \cdot \mu_{minima}^r + b_\iota \cdot \mu_{capsid}^r + c_\iota)$$

where σ is the standard sigmoid or threshold function used in neural networks. The training data are obtained from mutagenesis experiments that measure the effect of removing an interaction r on capsid assembly.

In addition, we learn the relative weights of the two scales through a scalar parameter $w_\iota \in [0, 1]$ which represents the importance of an interface type ι to any connectivity pathway. The probability of breaking a

connectivity pathway when an interaction is dropped is approximated by the equation:

$$C_p^r = 1 - \prod_{\iota \in p} (1 - w_\iota \cdot P_\iota^r) \tag{9}$$

For example, when $w_\iota = 0$, the corresponding term in Eq. 9 vanishes, and breaking any interface of type ι has no effect on disrupting assembly. Conversely, when all w_ι are equal, the probability of disruption depends only on P_ι^r 's, namely the cruciality of the interactions to interfaces and the number of connectivity paths in which an interface participates.

Putting these together, we get the *cruciality of an interaction r for capsid assembly* given by

$$H(r) = \sum_p C_p^r$$

In this model, the parameters a_ι , b_ι , c_ι , and w_ι are all unknown. We determine their value using simple machine learning. For a given partial order over the interactions $T = \{(r_i, r_j) : r_i \text{ has bigger impact on the capsid assembly than } r_j\}$, the impact function should satisfy $H(r_i) > H(r_j)$. Towards this end, we design a loss function:

$$L = \sum_{(r_i, r_j) \in T} \sigma(H(r_i) - H(r_j))$$

where S is the standard sigmoid or threshold function used in neural networks. When the cruciality function H satisfies the partial order, the loss function will be minimal. So the parameters can be determined by evaluating

$$\arg \min_{a_\iota, b_\iota, c_\iota, w_\iota} L$$

Results validating these predictions are shown in Section 3.3.

3 Results

Section 3.1 describes the setup for both the mutagenesis and the computational experiments. Section 3.2 describes the results validating interaction cruciality prediction assuming that all interface types are equally important and is based only on the cruciality for interface assembly. Section 3.3 describes the results validating the two-scale prediction combining the interaction cruciality at the interface-scale and the interface cruciality at the capsid-scale using a statistical model.

3.1 Experimental setup

We obtain our prediction for $T = 1$ (AAV2 and MVM) and $T = 3$ (BMV) viral capsids, using wet-lab mutagenesis experiments for training and validation. In a mutagenesis experiment, candidate interactions are disabled by mutating one of the participating residues. This disables interactions involving all atoms in the residue.

The effect of the mutation on assembly efficacy was determined by measuring concentration of successfully assembled viral capsids via cryo-electron microscopy. The residues were classified by the yield of successfully assembled capsid compared to wild type after the mutation: a yield of 100% indicates that mutation has no affect on the assembly and the residue is marked *non-disrupt*; a yield of 0% indicates the assembly is completely disrupted, and the residue is marked as *disrupt*.

For the interface-scale prediction, we started from simplified potential energies designed from known X-ray structure of the coat protein monomers of each of the viruses and all their interfaces [30,31] (data provided by Mavis Agbandje-Mckenna’s lab). We treated the participating monomers or dimers as single rigid motifs in the interface assembly systems.

The potential energy includes the hard-sphere potential between all atom pairs (one from each participating monomer or dimer) with the Van der Waals radius set to 1.2 Å. We used Lennard-Jones pair potentials, setting

the energy difference of Eq. 4 to $E_h - E_l = 0.997kJ/Mol$ [32], and the weight in Eq. 5 to $w(N_a) \approx 1.5^{N_a}$. An implicit solvent was assumed.

Although, theoretically, the potential energy should include the Lennard-Jones potential of all atom pairs, only the set of atom pairs that are close enough to interact and are conserved in related viruses have noticeable contribution to the configurational entropy. For the different types of interfaces (3 types for $T = 1$ and 7 types for $T = 3$), we determined such pairs of interacting residues (10-20 pairs for each interface), called the *candidate interactions* of each interface.

Interface assembly landscapes were atlased using EASAL by inputting the X-ray 3D structures of the participating monomers and dimers and the above described pair potentials. Altogether 9 such atlases were obtained for each of the $T = 1$ interface assembly systems and 31 such atlases for the $T = 3$ as described in Section 2.4. Computations of cruciality required modification and analysis of each atlas for each interaction (approximately 20 per interface). Furthermore, we took into account the simultaneous disabling of all interactions involving a residue, as occurs in mutagenesis experiments.

In all cases, the interface-scale predictions were performed blindly without knowledge of experimental results concerning assembly-driving interactions. In particular, for AAV2, mutagenesis results were only obtained subsequent to the interface-scale predictions. For MVM and BMV, the experimental results were gathered from multiple sources. For the training phase of the second two-scale prediction, less than half of the mutagenesis results were used, picking pairs of interactions marked disrupt and non-disrupt.

3.2 Validating interface-based cruciality prediction

As discussed in the methods Section 2.4, for each interface assembly system s , we use the unweighted versions of the cruciality bar-code ($\mu_{minima}^{r,s}, \mu_{capsid}^{r,s}$) to predict the cruciality of an interaction to an interface. Fig. 8(a) shows the plot of of the these two parameters for the interface assembly system s being the 5-fold interface with monomers for BMV. Each row shows $\mu_{minima}^{r,s}, \mu_{capsid}^{r,s}$ and their ratio in two BMV 5-fold interface assembly systems (shown at the bottom right) where the interaction r (which is the row label) is removed. The row labeled ‘None’ is the *wild type* assembly system where no interaction has been removed. The wild type system has been used to normalize the values of all the other rows. The rows are sorted according to the largest value of μ_{capsid}^r .

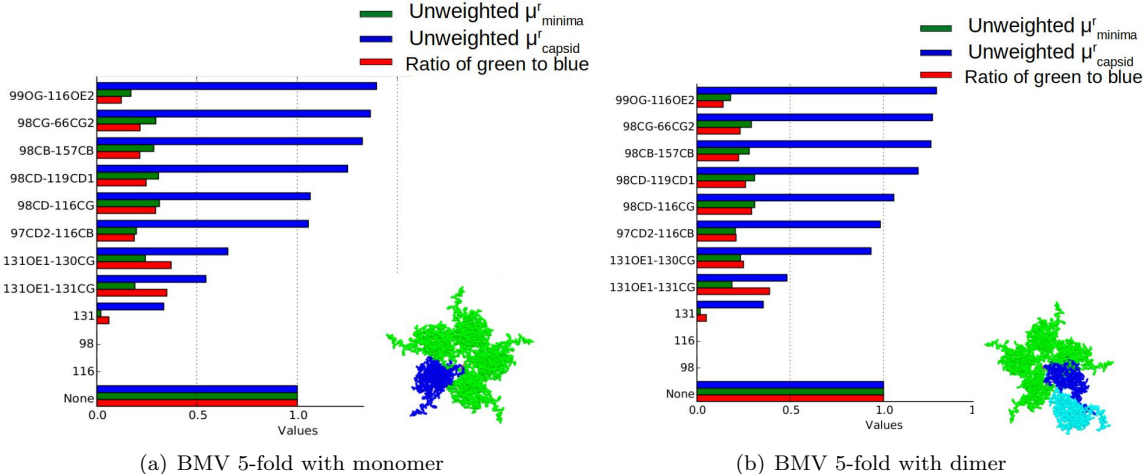


Fig 8. Cruciality bar-codes: each row shows $\mu_{minima}^r, \mu_{capsid}^r$ and their ratio in two BMV 5-fold interface assembly systems (monomer-monomer and monomer-dimer shown at bottom right) where the interaction r - listed as the row label - is removed. The row labeled ‘None’ is the “wild-type” assembly system where no interaction has been removed, whose ν_{minima} and ν_{capsid} values have been normalized. The rows are sorted according to the largest value of μ_{capsid}^r . See Section 3.2.

Fig. 8(b) plots the same parameters, but instead of considering monomers assembling at the 5-fold interface, we consider the assembly of a monomer and a dimer (as shown to the bottom right). As explained in Section 2.4, sterics play a larger role during the assembly of dimers than during the assembly of monomers. Note that certain interactions that had a lower value of μ_{capsid} in Fig. 8(a) have a higher value in Fig. 8(b). Since these plots merely illustrate our predictions without comparing them to mutagenesis data, the interested reader is referred to the link in the Section 6 for the complete set of such data, for all the interface assembly systems for all the viruses.

3.2.1 Validating the first two-scale prediction

Fig. 9 shows the cruciality bar-code of residues for those interface types (6 out of 13 interface types across the 3 viruses) for which there were sufficient wet-lab results for validation and for which we were able to obtain cruciality predictions (see Section 4. As explained in Section 2.4, the cruciality bar-code for an interface type is a cumulative value obtained from cruciality bar-codes computed for all the assembly systems at that interface.

Our interface-scale predictions were completely blind to the experimental data that were used for validation. Although generalizing an interface-scale prediction to the capsid level assumes the necessity of that interface for capsid assembly, our interface-scale predictions were validated successfully using mutagenesis data towards capsid assembly disrupt. However, since this interface-scale prediction was part of a second prediction (Section 2.5) using statistical learning, that training data have been removed from Fig. 9.

The cruciality bar-code for each residue is marked by the mutagenesis result indicating whether it disrupts assembly or not. The blue convex hull delineates the residues that are shown to disrupt, the red convex hull delineates the residues that are shown to not disrupt. Yellow delineates outliers. The separation between the convex hulls as seen in these plots validates our predictions.

For a reader interested in independently running the EASAL software to reproduce our predictions, or in using other sources of experimental data to check our predictions, we refer to the link in the Section 6 containing a complete set of such cruciality bar-code plots, individually for all the interface assembly systems, as well as the cumulative values for all the interface types, for the 3 viruses.

To compensate for the paucity of wet-lab results, and to mitigate possible bias introduced when picking the candidate interactions, we added 2 more candidate interactions to each interface. These interactions are unlikely to be crucial, since they were not conserved across similar viruses. Atlases were regenerated for each interface assembly system, with these additional interactions and the cruciality bar-codes were computed for all interactions using the new atlases. The results for the two $T = 1$ viruses are shown as the last 4 figures of Fig. 9. Overall the added residues (red convex hull) fall outside the blue convex hull delineating the residues shown to disrupt assembly.

3.3 Validating the second two-scale prediction

Fig. 10 shows, for AAV, MVM and BMV, residues with their cruciality at the capsid-scale, calculated using the statistical model of Section 2.5. Residues listed on the top of the table are predicted as more crucial, and the ones listed lower are predicted as less crucial. Mutagenesis result are used to mark residues by color. Blue indicates the residue disrupts assembly, while red indicates that the residue does not disrupt assembly. Our predictions match up the mutagenesis data in most of the cases.

4 Discussion

We predict crucial inter-atomic interactions between monomers for the assembly of icosahedral viral capsids in 3 viruses. The crucial interaction prediction at the interface-scale uses an atlas (computed using the EASAL methodology) to approximate the changes in the partition function of the capsid. The prediction of interface cruciality at the capsid scale uses an approximation of combinatorial entropy. We use two 2-scale methods to predict interface cruciality at the capsid scale.

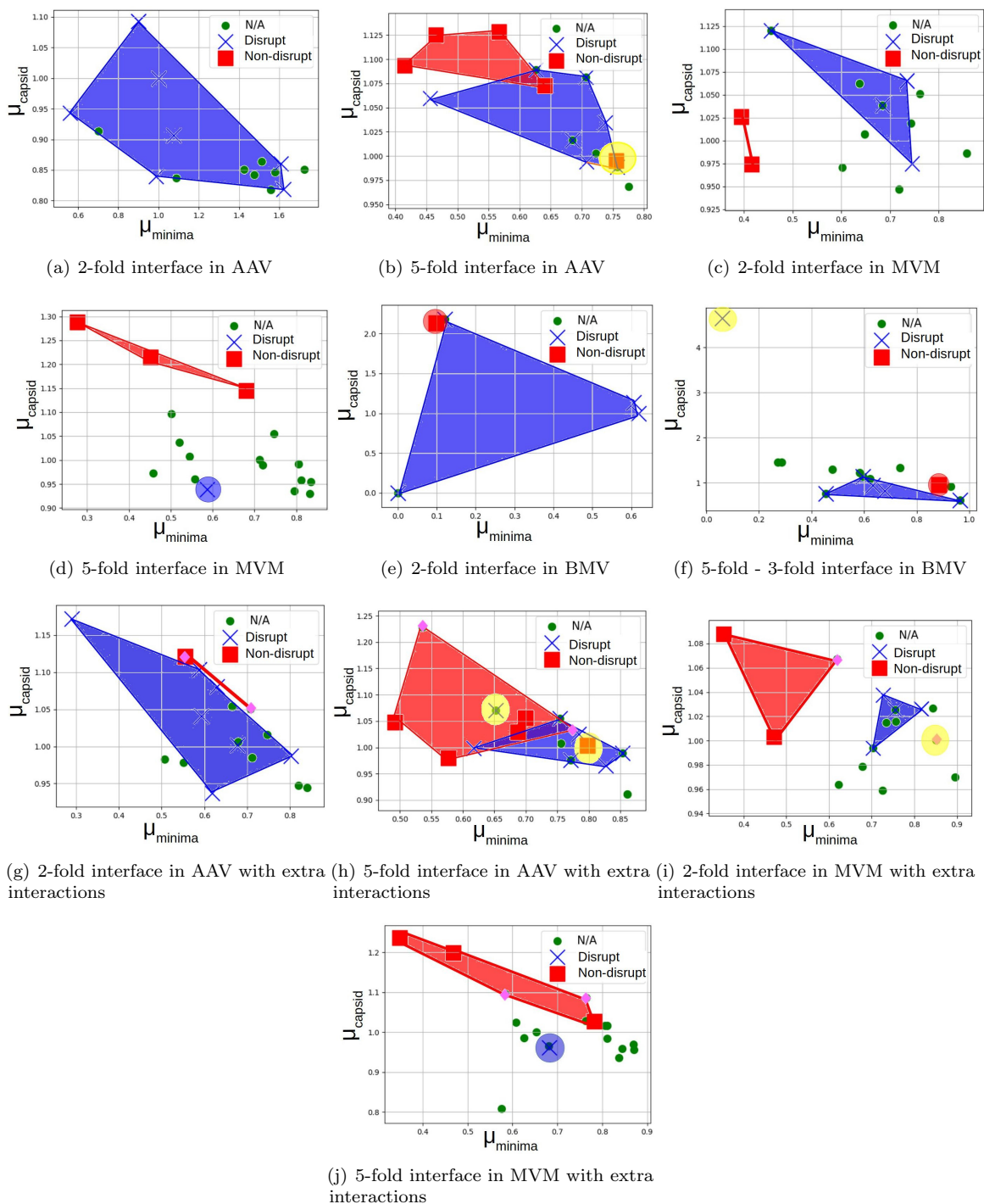


Fig 9. 2D plot of cruciality bar-codes for each interface. The blue convex hull delineates the residues that are shown to disrupt, the red convex hull delineates the residues that are shown to not disrupt the assembly process, yellow convex hull delineates the outliers. In (g)-(j), the pink diamonds are the extra interactions that were added to test for biases arising due to the paucity of mutagenesis data. See Section 3.2.1.

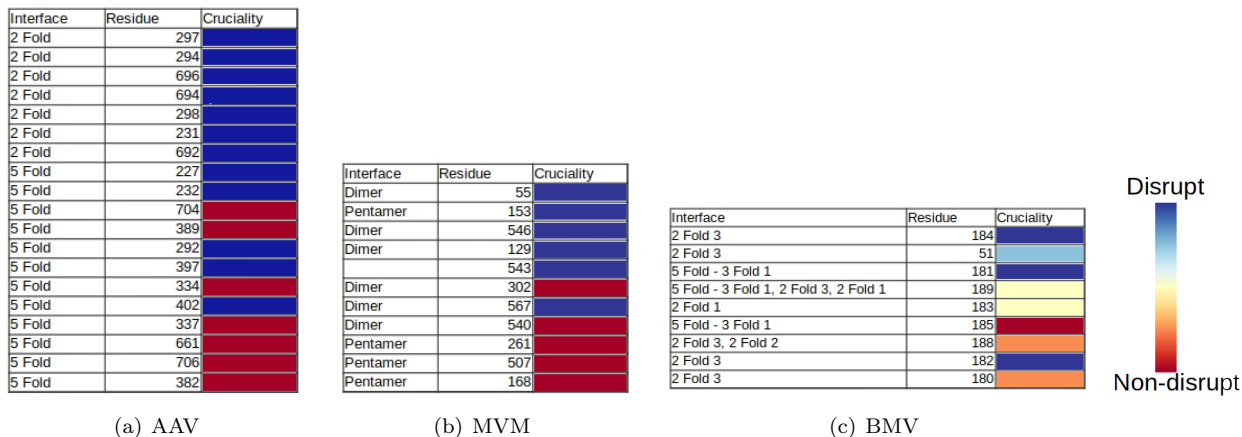


Fig 10. Cruciality prediction of residues for (a) AAV, (b) MVM, and (c) BMV. Cruciality of residues generated by the statistical model. The residue listed higher in the table are predicted as more crucial and the ones lower in the table are predicted as less crucial. Mutagenesis results are used to mark all the residues by color. Blue indicates that the residue disrupts assembly while red indicates that it does not. See Section 3.3.

There are several observations we made during the development of the method that may lead to future work.

Extra interactions The candidate interactions that serve as the input to EASAL are hand picked and pre-screened. Some interactions are excluded because they are not likely to be crucial based on some prior experience and some are excluded since no mutation on that residue is possible for now. This could potentially introduce bias in that the picked interactions are already likely more crucial than the others. In addition, since other non-crucial interactions also contribute to the potential energy, ignoring them will change the energy landscape. For better analysis, an extended set of candidate interactions should be used as the input to our method. This however is challenging, since the mutagenesis experiments in this paper took at least 2 years.

Rigidity of the 3 and 5 fold interfaces As explained in Section 2.1, we decompose the viral capsids into bi-assembly sub-systems consisting of two neighboring monomers or dimers. However, for the 3 and 5 folds interface, the rigidity properties of these subassemblies depend on not just the two monomers or dimers, but on all the monomers or dimers involved. Thus, to analyze these interfaces, we need to decompose the assembly system into tri-assembly and pent-assembly subsystems respectively. This would involve using new variants of EASAL that handle more than two input monomers [6]. We expect better prediction using the analysis of the complete multi-fold system.

Omitted interfaces Our results in Section 3.2 do not show the prediction results for interface cruciality for all interface types. Some of these left out interfaces did not have mutagenesis results for validation, and have been included in the link in Section 6. However, there are some interfaces that are not shown in the supporting information as well, since we were unable to get any useful predictions for these interfaces. These include the 3-fold interfaces for $T = 1$, $T = 3$ virus and some 2-fold interfaces for $T = 3$.

For 3-fold interfaces in AAV, we could not obtain useful cruciality bar-codes or rankings due to the heavy influence of sterics caused by interdigitation. In addition, mutagenesis of the 3-fold interface interactions did not disrupt assembly. We do not believe that the removal of any of the 3-fold interactions causes assembly disruption. Most of the residues in the 3-fold interface of BMV cross-link to the RNA and hence have no effect on assembly. We conjecture that in these cases, the assembly proceeds primarily by 2-fold and 5-fold interface interactions. Trimer interdigitation contributes to post-assembly stability of the capsid.

5 Conclusion

In this paper we predict crucial inter-atomic interactions between monomers for the assembly of icosahedral viral capsids in 3 viruses. The crucial interaction prediction at the interface-scale uses an atlas generated with minimal sampling using the EASAL geometric methodology that relies on convexifying landscape regions using Cayley parameters. From the atlas, a cruciality bar-code approximates the changes in the partition function of the capsid assembly landscape when an interaction is removed. At the capsid-scale, an approximation of combinatorial entropy is used to predict the cruciality of interface types at the capsid scale. We use 2 two-scale methods to predict interface cruciality at the capsid scale. The first method is entirely blind to known wet-lab experimental results, and assumes that each interface type is equally important for capsid assembly and only uses interaction cruciality at the interface scale to predict interaction cruciality at the capsid scale. The second method takes the variation among interface types into account, using statistical learning to relatively weight the predictions at the two scales. Mutagenesis results are used to validate our predictions. The method, being computationally lightweight, rapid, rigorous and reliable, could be used to narrow down the field of candidate assembly-driving interactions for wet-lab experiments as well as more computationally intensive in-silico experiments. For reproducibility, the reader can access and run the EASAL source code [1] with the help of descriptive papers [5,6], user guide [3] and video tutorial [2] as well as all of our raw prediction data for cruciality bar-codes at URL <https://geoplexity.bitbucket.io/virusSuppInfo.html>. This data includes EASAL predictions that could not be validated with the mutagenesis data we had access to, but could be checked against future mutagenesis experiments. At the interface-scale, the method is general enough to apply to any assembly system, in particular those that occur at various stages of the viral life-cycle, or during the action of tests and drugs.

6 Supporting information

Supporting information including raw prediction data for cruciality bar-codes, and ranking of residues which currently do not have mutagenesis data for validation, are available at <https://geoplexity.bitbucket.io/virusSuppInfo.html>.

Acknowledgments

This research was supported in part by NSF Grants DMS-0714912, CCF-1117695, DMS-1563234, and DMS-1564480.

References

1. Ozkan A, Prabhu R, Baker T, Pence J, Sitharam M. Efficient Atlasing and Search of Assembly Landscapes (ACM TOMS version); 2016. Available from: <https://bitbucket.org/geoplexity/easal>.
2. Prabhu R, Baker T, Sitharam M. Video Illustrating the opensource software EASAL; 2016. Available from: <https://cise.ufl.edu/~sitharam/EASALvideo.mpeg>.
3. Prabhu R, Sitharam M. EASAL software user guide.; 2016. Available from: <https://bitbucket.org/geoplexity/easal/src/master/CompleteUserGuide.pdf>.
4. Ozkan A, Sitharam M. EASAL: Efficient Atlasing, Analysis and Search of Molecular Assembly Landscapes. In: Proceedings of the ISCA 3rd International Conference on Bioinformatics and Computational Biology. BICoB-2011; 2011. p. 233–238.

5. Ozkan A, Prabhu R, Baker T, Pence J, Peters J, Sitharam M. Algorithm 990: Efficient Atlasing and Search of Configuration Spaces of Point-Sets Constrained by Distance Intervals. *ACM Trans Math Softw.* 2018;44(4):48:1–48:30. doi:10.1145/3204472.
6. Prabhu R, Sitharam M, Ozkan A, Wu R. Atlasing of assembly landscapes using distance geometry and graph rigidity; 2020. Available from: <https://arxiv.org/abs/1203.3811>.
7. Sitharam M, Agbandje-Mckenna M. Modeling virus self-assembly pathways: avoiding dynamics using geometric constraint decomposition. *Journal of Computational Biology.* 2006;13(6):1232–1265.
8. Sitharam M, Bóna M. Counting and Enumeration of Self-Assembly Pathways for Symmetric Macromolecular Structures. In: *Advances In Bioinformatics And Its Applications.* World Scientific; 2005. p. 426–436.
9. Bóna M, Sitharam M. The influence of symmetry on the probability of assembly pathways for icosahedral viral shells. *Computational and Mathematical Methods in Medicine.* 2008;9(3-4):295–302.
10. Bóna M, Sitharam M, Vince A. Enumeration of viral capsid assembly pathways: Tree orbits under permutation group action. *Bulletin of mathematical biology.* 2011;73(4):726–753.
11. Sitharam M. In: Jonoska N, Saito M, editors. *Modeling Autonomous Supramolecular Assembly.* Berlin, Heidelberg: Springer Berlin Heidelberg; 2014. p. 197–216. Available from: https://doi.org/10.1007/978-3-642-40193-0_9.
12. Karplus M, Kushick JN. Method for estimating the configurational entropy of macromolecules. *Macromolecules.* 1981;14(2):325–332. doi:10.1021/ma50003a019.
13. Andricioaei I, Karplus M. On the calculation of entropy from covariance matrices of the atomic fluctuations. *The Journal of Chemical Physics.* 2001;115(14):6289–6292.
14. Zhou HX, Gilson MK. Theory of Free Energy and Entropy in Noncovalent Binding. *Chemical Reviews.* 2009;109(9):4092–4107. doi:10.1021/cr800551w.
15. Hensen U, Lange OF, Grubmüller H. Estimating absolute configurational entropies of macromolecules: The minimally coupled subspace approach. *PloS one.* 2010;5(2).
16. Fogolari F, Corazza A, Fortuna S, Soler MA, VanSchouwen B, Brancolini G, et al. Distance-based configurational entropy of proteins from molecular dynamics simulations. *PLoS One.* 2015;10(7).
17. Huang D, Caflisch A. The free energy landscape of small molecule unbinding. *PLoS computational biology.* 2011;7(2).
18. Dunton TA, Goose JE, Gavaghan DJ, Sansom MS, Osborne JM. The free energy landscape of dimerization of a membrane protein, NanC. *PLoS computational biology.* 2014;10(1).
19. Staneva I, Wallin S. Binding free energy landscape of domain-peptide interactions. *PLoS computational biology.* 2011;7(8).
20. Prada-Gracia D, Gómez-Gardeñes J, Echenique P, Falo F. Exploring the free energy landscape: from dynamics to networks and back. *PLoS computational biology.* 2009;5(6).
21. Chirikjian GS. Chapter four - Modeling Loop Entropy. In: Johnson ML, Brand L, editors. *Computer Methods, Part C.* vol. 487 of *Methods in Enzymology.* Academic Press; 2011. p. 99 – 132.
22. Schwartz R, Shor PW, Prevelige Jr PE, Berger B. Local rules simulation of the kinetics of virus capsid self-assembly. *Biophysical journal.* 1998;75(6):2626–2636.

23. Berger B, Shor PW, Tucker-Kellogg L, King J. Local rule-based theory of virus shell assembly. *Proceedings of the National Academy of Sciences*. 1994;91(16):7732–7736.
24. Berger B, Shor PW. *The Mathematics of Virus Shell Assembly*. MIT Center for Advanced Education Services; 1994.
25. Berger B, Shor PW. Local rules switching mechanism for viral shell geometry. In: *Proc. 14th Biennial Conference on Phage Virus Assembly*. Citeseer; 1995.
26. Schwartz R, Prevelige Jr PE, Berger B. Local rules modeling of nucleation-limited virus capsid assembly. *Massachusetts Institute of Technology, Cambridge, MA*. 1998;.
27. Polles G, Indelicato G, Potestio R, Cermelli P, Twarock R, Micheletti C. Mechanical and assembly units of viral capsids identified via quasi-rigid domain decomposition. *PLoS computational biology*. 2013;9(11).
28. Pandey S, Johnson D, Kaplan R, Klobusicky J, Menon G, Gracias DH. Self-assembly of mesoscale isomers: the role of pathways and degrees of freedom. *PloS one*. 2014;9(10).
29. Sitharam M, St John A, Sidman J. *Handbook of Geometric Constraint Systems Principles*. 1st ed. CRC Press; 2018.
30. Agbandje-McKenna M, Llamas-Saiz A, Wang F, Tattersall P, Rossmann M. Functional implications of the structure of the murine parvovirus, minute virus of mice. *Structure*. 1998;6:1369–1381.
31. Padron E, Bowman V, Kaludov N, Govindasamy L, Levy H, Nick P, et al. Structure of adeno-associated virus type 4. *Journal of virology*. 2005;79(8):5047–58. doi:10.1128/JVI.79.8.5047-5058.2005.
32. Rahman A. Correlations in the Motion of Atoms in Liquid Argon. *Phys Rev*. 1964;136:A405–A411. doi:10.1103/PhysRev.136.A405.